Journal of Statistical Physics, Vol. 60, Nos. 5/6, 1990

Monte Carlo Study of the Ising Model Phase Transition in Terms of the Percolation Transition of "Physical Clusters"

Marco D'Onorio De Meo,[1] Dieter W. Heermann,[1,2] and Kurt Binder[1]

Received May 2, 1989; final October 17, 1989

Finite square $L \times L$ Ising lattices with ferromagnetic nearest neighbor interaction are simulated using the Swendsen–Wang cluster algorithm. Both thermal properties (internal energy U, specific heat C, magnetization $\langle |M| \rangle$, susceptibility χ) and percolation cluster properties relating to the "physical clusters," namely the Fortuin–Kasteleyn clusters (percolation probability $\langle P_\infty \rangle$, percolation susceptibility χ_p, cluster size distribution n_l) are evaluated, paying particular attention to finite-size effects. It is shown that thermal properties can be expressed entirely in terms of cluster properties, $\langle P_\infty \rangle$ being identical to $\langle |M| \rangle$ in the thermodynamic limit, while finite-size corrections differ. In contrast, χ_p differs from χ even in the thermodynamic limit, since a fluctuation in the size of the percolating net contributes to χ, but not to χ_p. Near T_c the cluster size distribution has the scaling properties as hypothesized by earlier phenomenological theories. We also present a generalization of the Swendsen–Wang algorithm allowing one to cross over continuously to the Glauber dynamics.

KEY WORDS: Percolation; "physical clusters"; Ising model; Monte Carlo simulation; finite-size scaling; Fortuin–Kasteleyn representation; Swendsen–Wang algorithm.

1. INTRODUCTION AND OVERVIEW

It has been a long-standing idea that the growth of correlations in a statistical mechanical system approaching a critical point ought to be describable in terms of some sort of "physical clusters."[1–6] The critical

[1] Institut für Physik, Johannes Gutenberg-Universität Mainz, Postfach 3980, West Germany.
[2] Also at Fachbereich Physik, Universität Wuppertal, D-5600 Wuppertal, West Germany. Permanent address: Institut für Theoretische Physik, Universität Heidelberg, 6900 Heidelberg, West Germany.

0022-4715/90/0900-0585$06.00/0

exponents describing the critical singularities of thermal properties at the second-order transition would then be related to the critical exponents describing the size distribution of "physical clusters"; and the spontaneous order appearing below the critical temperature T_c would be related to the formation of an "infinite cluster," i.e., at T_c a percolation transition[7] would occur where an infinite percolating network has been formed. But for many years it was unclear how to define "physical clusters" having these properties.

Of course, the prototype model for which this nice but qualitative idea should be made precise is the two-dimensional Ising model, for which so much exact knowledge has been accumulated.[8] Initially it has been thought[1,9,10] that "physical clusters" in the Ising model can be defined simply in geometrical terms of the spin configuration: a group containing l overturned spins, where each down spin has at least one other down spin as a nearest neighbor, separated from the surrounding up spins by a closed contour, is called an l-cluster. Denoting the average number of l-clusters per lattice site as n_l, the magnetization then can be exactly written as ($\langle \cdots \rangle$ stands for a thermal average)

$$\langle |M| \rangle = 1 - 2 \sum_{l=1}^{\infty}{}' l n_l \tag{1}$$

where the prime indicates that an infinite cluster (if it occurs) has to be omitted from the summation. Of course, the above qualitative description implies that for $T \leqslant T_c$ only the up spins are percolating, while at T_c an incipient percolating cluster of down spins occurs.

In spite of early numerical evidence[9,10] for this geometrical cluster (or "contour cluster") definition, it now is clear that these geometrical clusters *cannot be identified with the physical clusters* describing a thermal phase transition:

(i) For the three-dimensional Ising model, the geometrical clusters percolate already at a temperature $T_p \approx 0.96 T_c$ [11,12] before thermal criticality is reached. The thermal properties at this temperature show no singularity whatsoever. Despite much effort,[13–15] the properties of the size distribution of the geometrical clusters near T_c in the three-dimensional Ising model are not fully understood.

(ii) In the two-dimensional Ising model, topological considerations imply that the percolation transition of geometrical clusters and the thermal critical point must coincide.[5] But while the mean size of "physical clusters" (expressed by the "percolation susceptibility") χ_p

$$\chi_p = \sum_{l=1}^{\infty}{}' l^2 n_l \tag{2}$$

ought to diverge for $T \to T_c$ proportional to the thermal susceptibility $\chi_T \sim (1 - T/T_c)^{-\gamma}$, it can be shown by series expansions[16] that $\chi_p \sim (1 - T/T_c)^{-\gamma_p}$ with $\gamma_p > \gamma$.

(iii) It is not obvious how to explicitly incorporate the up–down symmetry of the Ising model above T_c in the absence of symmetry-breaking fields into the cluster description.[2,3]

Having accepted the fact that the geometrical clusters are on average larger than the "physical clusters" hopefully describing critical correlations, some prescription must be found by which the geometrical clusters are cut into pieces of suitable size, so that they describe the strongly correlated parts of order parameter fluctuations.[3,17] While early phenomenological scaling theories[3,17] have assumed the existence of this prescription to define "physical clusters" without being able to specify it explicitly, the first explicit construction of "physical clusters" from geometrical ones was proposed by Coniglio and Klein.[4] They suggested to distinguish between active and inactive bonds in a geometrical cluster, with the probability for a bond to be active given by

$$p = 1 - \exp(-2J/k_B T) \tag{3}$$

where J is the exchange constant. Now only sites connected by active bonds form a "physical cluster." A geometrical cluster thus can consist of several "physical clusters," which are disconnected from each other. Equation (3) can be shown[4] to ensure that the percolation threshold and the critical point coincide, and at the same time the connectedness length ξ_p is proportional to ξ_T, and also $\chi_p \sim \chi_T$ in this model.

However, as it stands, the prescription[3] of Coniglio and Klein[4] applies to the down spins only, and the problem (iii) of the description of the paramagnetic phase remains.

Parallel to this research activities, a quite independent strand of thought developed beginning 1969 with the work of Fortuin and Kasteleyn.[24] They introduced a correlated bond-percolation model (the random-cluster model) indexed by a real parameter q, and proved identities relating the partition function and connectedness probabilities in this model (when $q = 2, 3, \ldots$) to the partition function and correlation functions of the q-state Potts model. These identities imply, for example, that the susceptibility of the Ising model is equal to the mean cluster size in the $q = 2$ random cluster model.

Hu,[6] on the basis of this result, suggested to apply active or nonactive bonds between all pairs of parallel spins, irrespective of whether they point up or down, using again Eq. (3). Then problem (iii) is taken care of.

Swendsen and Wang[23] finally developed a new algorithm which

intrinsically constructs these clusters. The relation between these two strands of thought merging to the new algorithm and to the results of this work have recently been made very clear in a work of Edwards and Sokal.[38]

While the work of Coniglio and Klein[4] and Hu[6] proves for the "physical clusters" the equivalence of the critical exponents of the percolation quantities $\{\langle |P_\infty| \rangle, \chi_p$ and $\xi_p\}$ and the critical exponents of the corresponding thermal quantities $\{\langle |M| \rangle, \chi_T$ and $\xi_T\}$, nothing is said by in refs. 4 and 6 about the critical amplitudes, and the behavior outside the critical region. Furthermore, the detailed cluster size distribution has not been studied, and the phenomenological scaling theory for "physical clusters"[3] has not been tested. In a preliminary communication, Binder and Heermann[18] applied standard Monte Carlo techniques[19–22] to study the cluster size distribution for the two-dimensional Ising model at $T=0.9T_c$. It was found that qualitatively similar behavior of n_l as a function of l occurs for geometrical clusters and for "physical clusters" (according to both the Coniglio-Klein[4] and Hu[6] definitions). This observation makes plausible why the geometrical cluster distribution studied by Stoll *et al.*[9] could be fitted to the Fisher[1] cluster model, which is an approximate[3] description of "physical clusters" only. However, neither the temperature dependence of n_l nor finite-size effects have been analyzed yet.

In fact, applying standard Monte Carlo methods, this task would be rather difficult, since a large number of statistically independent spin configurations is needed to sample the (small) concentrations n_l for large cluster sizes l with sufficient statistics, and this is hampered by the strong "critical slowing down" of the standard algorithms. For this purpose, the algorithm due to Swendsen and Wang[23] is very advantageous, since it strongly reduces this correlation due to "critical slowing down"; and for implementing the algorithm, all the information on "physical clusters" has to be generated anyway. Hence, we have used this algorithm for our investigation throughout; we briefly review it and its theoretical foundation in the next section. Section 3 then answers the questions posed above, providing explicit relations which link the thermal properties to their percolation counterparts. Section 4 describes our corresponding numerical results, and also presents a finite-size scaling analysis. Section 5 then presents the cluster size distribution n_l, also paying particular attention to the contribution from the largest clusters in the system. Finally, Section 6 summarizes a few conclusions and points out directions of future work.

2. THE SWENDSEN–WANG[23] ALGORITHM AND ITS FOUNDATION DUE TO THE FORTUIN–KASTELEYN[24] MAPPING

In this section we briefly review the theoretical foundations of the Swendsen–Wang algorithm, which is based intrinsically on the construction of clusters. In order to get an easy approach to the connection of Fortuin and Kasteleyn's work to the Swendsen–Wang algorithm and the problem of how to define appropriate "physical clusters," we will not use their original notations, but a form which directly shows up the transition probabilities from one state to another and was first proposed by Sokal and Edwards.[38] Then it will be easy to extend their original treatment to allow for arbitrary cluster definitions depending on a set $\{x_{ij}\}$ of parameters, $0 \leqslant x_{ij} \leqslant 1$.

Given a lattice with Potts spins $\sigma_i = 1,..., q$ on the sites and bond variables $n_{ij} = 0$ (open), 1 (closed) on the edges, we define the joint probability of a certain realization of Potts and bond variables as

$$P(\sigma, n) = Z^{-1} \prod_{\langle i,j \rangle} [(1 - p_{ij})\, \delta_{n_{ij},0} + p_{ij} \delta_{\sigma_i \sigma_j} \delta_{n_{ij},1}] \tag{4}$$

with

$$Z = \sum_{\sigma} \sum_{n} \prod_{\langle i,j \rangle} [(1 - p_{ij})\, \delta_{n_{ij},0} + p_{ij} \delta_{\sigma_i \sigma_j} \delta_{n_{ij},1}] \tag{5}$$

The p_{ij} are given by the couplings J_{ij} between the spins, $p_{ij} = 1 - \exp(-J_{ij})$, $\sigma = \{\sigma_i\}$, and $n = \{n_{ij}\}$. This is the so called FKSW model (Fortuin–Kasteleyn–Swendsen–Wang model) of ref. 38. Summation over all bond configurations yields

$$\begin{aligned} P(\sigma) &= \sum_{n} P(\sigma, n) \qquad (6) \\ &= Z^{-1} \prod_{\langle i,j \rangle} \sum_{n_{ij}=0}^{1} [(1 - p_{ij})\, \delta_{n_{ij},0} + p_{ij} \delta_{\sigma_i \sigma_j} \delta_{n_{ij},1}] \\ &= Z^{-1} \prod_{\langle i,j \rangle} [(1 - p_{ij}) + p_{ij} \delta_{\sigma_i \sigma_j}] \\ &= Z^{-1} \exp\left[- \sum_{\langle i,j \rangle} J_{ij} (1 - \delta_{\sigma_i \sigma_j}) \right] \\ &= Z^{-1} \exp[-H(\sigma)] \qquad (7) \end{aligned}$$

with $Z = \sum_{\sigma} \exp[-H(\sigma)]$, respectively, and $H(\sigma) = \sum_{\langle i,j \rangle} J_{ij}(1 - \delta_{\sigma_i \sigma_j})$ the Hamiltonian of the Potts model.

On the other hand, we can evaluate the sum over all spin configurations and obtain

$$P(n) = \sum_{\sigma} P(\sigma, n)$$

$$= Z^{-1} \sum_{\sigma} \left[\prod_{\langle ij \rangle, n_{ij}=1} p_{ij} \delta_{\sigma_i \sigma_j} \prod_{\langle ij \rangle, n_{ij}=0} (1 - p_{ij}) \right] \tag{8}$$

In the last expression all the terms in the sum with a closed bond between two spins in distinct states will vanish, so if we denote by σ^n a spin configuration compatible with the restriction for two spins to be parallel if connected by a closed bond, we get

$$P(n) = Z^{-1} \sum_{\sigma^n} \left[\prod_{\langle ij \rangle, n_{ij}=1} p_{ij} \prod_{\langle ij \rangle, n_{ij}=0} (1 - p_{ij}) \right]$$

The terms in the sum are now independent of the spin configuration. Given the bond configuration, the sum just counts the number of compatible spin configurations. If we define as a cluster the set of bond-connected spins, we get

$$P(n) = Z^{-1} \prod_{\langle ij \rangle, n_{ij}=1} p_{ij} \prod_{\langle ij \rangle, n_{ij}=0} (1 - p_{ij})\, q^{c(n)} \tag{9}$$

with q the number of possible spin orientations, e.g., Potts states, and $c(n)$ the number of clusters of the given bond configuration n. Equivalently,

$$Z = \sum_{n} \left[\prod_{\langle ij \rangle, n_{ij}=1} p_{ij} \prod_{\langle ij \rangle, n_{ij}=0} (1 - p_{ij})\, q^{c(n)} \right]$$

This is just the partition function of the random-cluster model introduced by Fortuin and Kasteleyn.[24]

For every joint probability we have the identities

$$P(\sigma, n) = P(\sigma \mid n)\, P(n) = P(n \mid \sigma)\, P(\sigma) \tag{10}$$

which imply the microreversibility condition. Now we can calculate the conditional probabilities to get from a bond configuration to a spin configuration and vice versa:

$$P(n \mid \sigma) = \frac{P(\sigma, n)}{P(\sigma)} = \prod_{\langle ij \rangle, \sigma_i = \sigma_j} \left[(1 - p_{ij})\, \delta_{n_{ij},0} + p_{ij} \delta_{n_{ij},1} \right] \prod_{\langle ij \rangle, \sigma_i \neq \sigma_j} \delta_{n_{ij},0} \tag{11}$$

is the probability to obtain the bond configuration n given the spin configuration σ. In the case $\sigma_i \neq \sigma_j$ only open bonds are allowed; in the case

$\sigma_i = \sigma_j$ a closed bond is put with probability p_{ij} and an open bond with probability $1 - p_{ij}$. We have

$$P(\sigma \mid n) = \frac{P(\sigma, n)}{P(n)} = q^{-c(n)} \prod_{\langle ij \rangle, n_{ij}=1} \delta_{\sigma_i, \sigma_j} \tag{12}$$

for the probability to obtain the spin configuration σ given the bond configuration n, flipping the $c(n)$ clusters of n independently in one of the q Potts states with the restriction the spins of one cluster to be in the same state.

The Swendsen–Wang algorithm is nothing but the repeated application of the two transition probabilities. We have immediately

$$P(\sigma') = \sum_{\sigma} T_{\sigma'\sigma} P(\sigma)$$

with

$$T_{\sigma'\sigma} = \sum_{n} P(\sigma' \mid n)\, P(n \mid \sigma)$$

describing a Markov chain with the canonical equilibrium distribution of the Potts model as eigenvector.

In the following treatment we will extend the FKSW model to allow for arbitrary cluster definitions. Let n_{ij} assume three values, $n_{ij} = -1, 0, 1$; we will denote them by saying n_{ij} is an energy, an open, or a closed bond, respectively. Let us further introduce a new set of real parameters x_{ij}, $0 \leqslant x_{ij} \leqslant 1$, and define an extended FKSW model:

$$\begin{aligned} P_e(\sigma, n) = Z_e^{-1} \prod_{\langle ij \rangle} \{ & (1 - p_{ij})[x_{ij} \delta_{n_{ij},0} + (1 - x_{ij})\, \delta_{n_{ij},-1}] \\ & + p_{ij} \delta_{\sigma_i \sigma_j} [x_{ij} \delta_{n_{ij},1} + (1 - x_{ij})\, \delta_{n_{ij},-1}] \} \end{aligned} \tag{13}$$

with

$$\begin{aligned} Z_e = \sum_{\sigma} \sum_{n} \prod_{\langle ij \rangle} \{ & (1 - p_{ij})[x_{ij} \delta_{n_{ij},0} + (1 - x_{ij})\, \delta_{n_{ij},-1}] \\ & + p_{ij} \delta_{\sigma_i \sigma_j} [x_{ij} \delta_{n_{ij},1} + (1 - x_{ij})\, \delta_{n_{ij},-1}] \} = Z \end{aligned}$$

In the case $x_{ij} = 1$, for all i, j we retain the original FKSW model.

It is now convenient to define a cluster surface energy, where a cluster is still defined as the set of all spins which are connected by a closed bond ($n_{ij} = 1$). For a given cluster there is a unique set of boundary bonds, e.g., bonds between a spin of the cluster and a spin not belonging to the cluster.

The boundary bonds of a cluster by definition are either energy or open bonds ($n_{ij} = -1, 0$). Let

$$E_{cl} = \tfrac{1}{2} \sum_{\langle ij \rangle_{cl}} J_{ij}(1 - \delta_{\sigma_i \sigma_j})\, \delta_{n_{ij}, -1}$$

be the associated cluster surface energy which is affected only by boundary energy bonds between spins in different states. The sum goes over all pairs $\langle i, j \rangle$ with at least one site belonging to the cluster. The total surface energy is then given by

$$E_s(\sigma, n) = \sum_{\text{all cluster}} E_{cl} = \sum_{\langle ij \rangle, n_{ij} = -1} J_{ij}(1 - \delta_{\sigma_i \sigma_j}) \tag{14}$$

The factor 1/2 cancels out by counting the boundary bonds twice in the first sum. With $p_{ij} = 1 - \exp(-J_{ij})$ we finally obtain

$$\exp[-E_s(\sigma, n)] = \prod_{\langle ij \rangle, n_{ij} = -1} [(1 - p_{ij}) + p_{ij} \delta_{\sigma_i \sigma_j}] \tag{15}$$

Performing the same calculations as for the initial FKSW model yields

$$P(\sigma) = \sum_n P_e(\sigma, n) = Z^{-1} \prod_{\langle ij \rangle} [(1 - p_{ij}) + p_{ij} \delta_{\sigma_i \sigma_j}] \tag{16}$$

and

$$\begin{aligned} P(n) &= \sum_\sigma P_e(\sigma, n) \\ &= Z^{-1} \left(\prod_{\langle ij \rangle, n_{ij} = 1} x_{ij} p_{ij} \right) \left[\prod_{\langle ij \rangle, n_{ij} = 0} x_{ij}(1 - p_{ij}) \right] \\ &\quad \times \left[\prod_{\langle ij \rangle, n_{ij} = -1} (1 - x_{ij}) \right] \\ &\quad \times \sum_\sigma \left\{ \prod_{\langle ij \rangle, n_{ij} = 1} \delta_{\sigma_i \sigma_j} \prod_{\langle ij \rangle, n_{ij} = -1} [(1 - p_{ij}) + p_{ij} \delta_{\sigma_i \sigma_j}] \right\} \end{aligned}$$

In the last sum all the terms involving configurations with connected spins not in the same state vanish, and with (15) we obtain

$$\begin{aligned} P(n) &= \sum_\sigma P_e(\sigma, n) \\ &= Z^{-1} \left(\prod_{\langle ij \rangle, n_{ij} = 1} x_{ij} p_{ij} \right) \left[\prod_{\langle ij \rangle, n_{ij} = 0} x_{ij}(1 - p_{ij}) \right] \\ &\quad \times \left[\prod_{\langle ij \rangle, n_{ij} = -1} (1 - x_{ij}) \right] \sum_{\sigma^n} \exp[-E_s(\sigma, n)] \end{aligned} \tag{17}$$

We also have

$$P(n|\sigma)=\frac{P(\sigma,n)}{P(\sigma)}=\prod_{\langle ij\rangle,\sigma_i=\sigma_j}[x_{ij}p_{ij}\delta_{n_{ij},1}+x_{ij}(1-p_{ij})\,\delta_{n_{ij},0}+(1-x_{ij})\,\delta_{n_{ij},-1}]$$
$$\times\prod_{\langle ij\rangle,\sigma_i\neq\sigma_j}[x_{ij}\delta_{n_{ij},0}+(1-x_{ij})\,\delta_{n_{ij},-1}] \tag{18}$$

which means that the probabilities to find an energy, an open, or a closed bond between parallel spins are $1-x_{ij}$, $x_{ij}(1-p_{ij})$, and $x_{ij}p_{ij}$, respectively, between spins in different states $(1-x_{ij})$, x_{ij}, 0. On the other hand, we obtain

$$P(\sigma|n)=\frac{P(\sigma,n)}{P(n)}=\frac{\exp[-E_s(\sigma,n)]}{\sum_{\sigma'}\exp[-E_s(\sigma',n)]}\prod_{\langle ij\rangle,n_{ij}=1}\delta_{\sigma_i\sigma_j} \tag{19}$$

i.e., the clusters defined by the bond configuration n are not independent, but their orientations have a statistical weight given by their surface energy. Be aware that for $x_{ij}=1$ for all $\langle i,j\rangle$ there are no energy bonds, so the surface energy vanishes and we have to count for the number of possible independent cluster orientations, which gives Eq. (12) again. This transition probability can easily be obtained by a standard Metropolis or heat-bath algorithm where each cluster is flipped due to the restriction that the energy has to be lowered or raised with a certain probability depending on the energy difference between the old and the new state. Again in the case $x_{ij}=1$ for all $\langle i,j\rangle$ there is no energy difference between different orientations of the clusters and we recover the Swendsen–Wang algorithm. On the other hand, if the x_{ij} are chosen to be zero for all $\langle i,j\rangle$, there exist only energy bonds, the clusters are reduced to the size of one spin, and we get the usual single-spin-flip dynamic of the standard Monte Carlo simulation. Varying the x_{ij} homogeneously from zero to one, the clusters will become larger and the surface energy will tend to zero, transforming into a "bulk" energy given by the number of closed bonds for the total energy remaining constant (see also the next section, where an explicit identity between the number of closed bonds and energy is given). The choice of the set x_{ij} does not affect the equilibrium behavior of the model, but the dynamics of the simulation, allowing for continuous variation between a local or more global dynamics. It is known[23,39,40] that the critical slowing down approaching the critical point can be lowered substantially by choosing a more global dynamics instead of a local dynamics. So this model allows for a systematic investigation of this effect. There is also the possibility for a mixed choice $x_{ij}=0,1$ for adapting the model to optimum parallelization, if one wishes to use parallel computers, dividing the whole system into identical subsystems where on the boundaries of these subsystems we

choose $x_{ij}=0$ for a minimum of information transfer between different processors, regarding only the orientation of the boundary spins, and $x_{ij}=1$ in the bulk of the subsystems in order to gain the acceleration due to the reduced critical slowing down.

Let us further remark that the above treatment also allows for the application of an external field by introducing a ghost spin connected by a series of bonds to the initial spins of the system. The couplings are then directly given by the strength of the applied field. Choosing, for example, the extended set $\{x_{ij}\}$ to allow for energy bonds only ($x_{ij}=0$) if connecting to the ghost spin and for closed or opened bonds otherwise ($x_{ij}=1$), the conventional Swendsen–Wang algorithm is obtained, where the clusters are flipped independently, but with different probabilities into different states, depending on the cluster size and the external field.[41]

In the following we restrict ourselves to the case $x_{ij}=1$ for all $\langle i, j\rangle$, giving some additional equalities between cluster coordinates and macroscopic observables in equilibrium due to the independence of the clusters which is essential for them to behave as "physical clusters," as will be shown explicitly in Section 3.

For convenience we investigate the two-dimensional Ising model on the square lattice with periodic boundary conditions, zero external field, and homogeneous interactions $J_{ij}=J$, using the conventional Ising Hamiltonian with $\sigma_i=-1, +1$ instead of $\sigma_i=1, 2$ in the Potts model,

$$\mathscr{H}=-J\sum_{\langle ij\rangle}\sigma_i\sigma_j \tag{20}$$

Note that this transformation of coordinates only gives rise to an energy shift of the total energy and a change of the coupling constants by a factor of 2.

The simulations are carried out by an implementation of the Swendsen–Wang algorithm; ref. 25 gives details on the simulation program. The cluster analysis is based on the Hoshen–Kopelman algorithm.[26] The program used in the following for $L=100$ reached a speed of generating about 7 system configurations per second (in comparison to a single spin flip algorithm this would correspond to 7×10^4 Monte Carlo steps/sec) on a SIEMENS 7561 scalar computer (which roughly corresponds in speed to an IBM 3081 machine). Despite serious efforts,[25] no efficiently vectorizing program code could be found, due to the complicated cluster analysis necessary for this algorithm. Thus, in spite of the conceptual advantage that the Swendsen–Wang algorithm[23] drastically reduces the correlations due to critical slowing down, for the linear dimensions L studied here ($L\leqslant100$) only modest gains in statistical accuracy of the numerical

results occur, as compared to standard vectorized Ising model simulation algorithms at supercomputers.[27,28] One can, however, parallelize the Swendsen–Wang algorithm.[29]

3. THERMAL PROPERTIES OF THE ISING MODEL EXPRESSED IN TERMS OF PHYSICAL CLUSTERS

In this section we consider internal energy, specific heat, magnetization, and susceptibility of the Ising model and use the cluster definition justified in the previous section to express these thermal properties by properties of the cluster distribution. Unlike the case of the geometrical cluster definition,[1,9] where only one cluster coordinate [the cluster size l; cf. Eq. (1)] matters, one needs two "cluster coordinates,"[3] relating to cluster magnetization $m_{cl} = l$ times the sign of the cluster orientation and the cluster energy, or equivalently the number u_{cl} of bonds in a cluster denoted by $\{cl\}$, divided by the bond probability p [Eq. (3)]. If the number of clusters (per lattice site) with magnetization m_{cl} and with $u_{cl}p$ bonds is $p(m_{cl}, u_{cl})$, we have the relation expressing the fact that every site must belong to some cluster

$$\sum_{m_{cl}} \sum_{u_{cl}} |m_{cl}|\, p(m_{cl}, u_{cl}) = 1 \tag{21}$$

It is also useful to define the reduced cluster distributions depending on one coordinate only,

$$p(m_{cl}) = \sum_{u_{cl}} p(m_{cl}, u_{cl}), \qquad p(u_{cl}) = \sum_{m_{cl}} p(m_{cl}, u_{cl}) \tag{22}$$

From Eq. (20) we obtain

$$\mathscr{H} = 2J(N - N_{\uparrow\uparrow}) \tag{23}$$

since on the square lattice there occur $2N$ bonds. For $\langle N_{\uparrow\uparrow} \rangle$ pairs of parallel spins the average number of bonds $\langle N_b \rangle$ is $\langle N_b \rangle = p\langle N_{\uparrow\uparrow} \rangle$, and thus the energy per spin $u = \langle \mathscr{H} \rangle / N$ can be written as

$$u = -2J\left(\frac{\langle N_b \rangle}{pN} - 1\right) \tag{24a}$$

or alternatively, in terms of $\langle p(u_{cl}) \rangle$,

$$u = -2J\left(\sum_{u_{cl}} u_{cl} \langle p(u_{cl}) \rangle - 1\right) \tag{24b}$$

The specific heat is found as

$$C=\frac{\partial\langle\mathscr{H}\rangle}{\partial T}=\frac{1}{k_{\mathrm{B}}T^2}(\langle\mathscr{H}^2\rangle-\langle\mathscr{H}\rangle^2)=\frac{4J^2}{k_{\mathrm{B}}T^2}(\langle N_{\uparrow\uparrow}^2\rangle-\langle N_{\uparrow\uparrow}\rangle^2) \tag{25}$$

where in the last step Eq. (23) was used. On the other hand, the first result of Eq. (25) implies, using Eq. (24a),

$$C=-2J\frac{\partial}{\partial T}\left(\frac{\langle N_b\rangle}{p}\right)=-\frac{2J}{p^2}\left(p\frac{\partial}{\partial T}\langle N_b\rangle-\langle N_b\rangle\frac{\partial}{\partial T}p\right) \tag{26}$$

Now the fluctuation relation for $\langle N_b\rangle$ analogous to Eq. (25) yields in Eq. (26) ($q=1-p$)

$$C=\frac{1}{k_{\mathrm{B}}T^2}\frac{4J^2}{p^2}(\langle N_b^2\rangle-\langle N_b\rangle^2-q\langle N_b\rangle) \tag{27}$$

Thus, it is seen that the heat capacity is not only due to the fluctuation in the number of bonds, but there is also a correction term due to the fact that p is temperature dependent. Clearly this correction term is non-vanishing in the thermodynamic limit.

It is instructive to calculate averages such as those involved in Eq. (25) directly from the general formalism of the previous section. For example, applying Eqs. (10) and (11), one finds

$$\begin{aligned}\langle N_b^2\rangle&=\sum_n P(n)\,N_b^2(n)\\&=\sum_\sigma P(\sigma)\sum_n P(n\,|\,\sigma)\,N_b^2(n)\\&=\sum_\sigma P(\sigma)\sum_n p^{N_b(n)}q^{N_{\uparrow\uparrow}(\sigma)-N_b(n)}\delta_{n,\sigma}N_b^2(n)\\&=\sum_\sigma P(\sigma)\sum_{N_b=0}^{N_b=N_{\uparrow\uparrow}(\sigma)}\binom{N_{\uparrow\uparrow}(\sigma)}{N_b}p^{N_b(n)}q^{N_{\uparrow\uparrow}(\sigma)-N_b(n)}N_b^2(n)\\&=\sum_\sigma P(\sigma)[p^2N_{\uparrow\uparrow}(\sigma)+pqN_{\uparrow\uparrow}(\sigma)]\\&=p^2\langle N_{\uparrow\uparrow}^2\rangle+pq\langle N_{\uparrow\uparrow}\rangle\end{aligned} \tag{28}$$

In this way Eq. (27) follows from Eq. (25), using once more $p\langle N_{\uparrow\uparrow}\rangle=\langle N_b\rangle$ and defining $\delta_{n,\sigma}=\prod_{\langle ij\rangle,\sigma_i\neq\sigma_j}\delta_{n_{ij}}$.

The magnetization per spin is written in terms of Eq. (22),

$$M=(1/N)\sum_i\sigma_i=\sum_{m_{cl}}m_{cl}\,p(m_{cl}) \tag{29}$$

We split off from $p(m_{cl})$ the contribution of the largest cluster in the system, which we denote as m_{cl}^{∞},

$$p(m_{cl}) \equiv p'(m_{cl}) + (1/N)\,\delta_{m_{cl},m_{cl}^{\infty}} \tag{30}$$

Note that for $T > T_c$ and finite N there may occur several clusters with the same value $|m_{cl}^{\infty}|$ in a configuration—the definition of Eq. (30) then requires that one of them arbitrarily is defined to be the largest cluster. If there are several clusters with the same value $|m_{cl}^{\infty}|$ but different sign, we choose for m_{cl}^{∞} the same sign as for M. Thus, we obtain

$$\langle |M| \rangle = \frac{1}{N} \left\langle \left| \sum_i \sigma_i \right| \right\rangle = \left\langle \left| \frac{m_{cl}^{\infty}}{N} + \sum_{m_{cl}} m_{cl}\, p'(m_{cl}) \right| \right\rangle \tag{31}$$

On the other hand, let $P_{\infty} = |m_{cl}^{\infty}|/N$ be the fraction of sites belonging to the largest cluster; its mean $\langle P_{\infty} \rangle$ is the percolation probability. Then we see that $\langle P_{\infty} \rangle$ and $\langle |M| \rangle$ differ in a finite system, due to a contribution of clusters other than the largest ones: we have $\langle |M| \rangle \geqslant \langle P_{\infty} \rangle$; the equality sign holds in the thermodynamic limit only. While $\langle \sum_{m_{cl}} m_{cl}\, p'(m_{cl}) \rangle = 0$, i.e., positive and negative values of the sum are equally probable, due to the absolute value in Eq. (31), $|M|$ on the average is larger than P_{∞}. This effect will be discussed more quantitatively in the next section.

Similar extra terms appear when we relate the thermal susceptibility to the percolation susceptibility. Writing for the thermal susceptibility the fluctuation relation (we use an expression which has the proper thermodynamic limit for $T < T_c$)[22,30]

$$k_B T \chi' = N(\langle M^2 \rangle - \langle |M| \rangle^2) \tag{32}$$

we split the sum over correlations into terms due to the same cluster and due to different clusters:

$$\langle M^2 \rangle = \frac{1}{N^2} \left\langle \sum_{i,j} \sigma_i \sigma_j \right\rangle = \frac{1}{N^2} \left\langle \sum_{\substack{i,j \\ \text{in the} \\ \text{same cluster}}} \sigma_i \sigma_j \right\rangle + \frac{1}{N^2} \left\langle \sum_{\substack{i,j \\ \text{in different} \\ \text{clusters}}} \sigma_i \sigma_j \right\rangle \tag{33}$$

Now the last sum in Eq. (33) vanishes, since different clusters are not correlated with each other per construction. Furthermore,

$$\left\langle \sum_{\substack{i,j \\ \text{in the} \\ \text{same cluster}}} \sigma_i \sigma_j \right\rangle = N \sum_{m_{cl}} m_{cl}^2 \langle p(m_{cl}) \rangle \tag{34}$$

Using again Eq. (30) to separate out the contribution of the largest cluster yields

$$k_B T\chi' = \sum_{m_{cl}} m_{cl}^2 \langle p'(m_{cl}) \rangle + N(\langle P_\infty^2 \rangle - \langle |M| \rangle^2) \tag{35}$$

For large systems and $T < T_c$ it is a very good approximation to replace $\langle |M| \rangle$ by $\langle P_\infty \rangle$, to obtain [$\sum_{m_{cl}} m_{cl}^2 \langle p'(m_{cl}) \rangle = \chi'_p$ as defined in Eq. (2)]

$$k_B T\chi' \approx k_B T\chi'^{(p)} = \chi'_p + N(\langle P_\infty^2 \rangle - \langle P_\infty \rangle^2) \tag{36}$$

Thus, the magnetic susceptibility has two contributions: the first one is due to the contribution of the clusters other than the largest ones, and this is the percolation susceptibility χ_p that is usually considered.[7] The second contribution is due to fluctuations on the size of the percolating network.

As discussed in more detail elsewhere,[22,30] it is a consequence of the fact that the Ising model has a spontaneously broken symmetry in the thermodynamic limit, while finite systems cannot exhibit symmetry breaking, that different fluctuation formula must be used to describe the zero-field susceptibility above T_c and below T_c: Above T_c, the expression replacing Eq. (32) is

$$k_B T\chi = N\langle M^2 \rangle = \sum_{m_{cl}} m_{cl}^2 \langle p(m_{cl}) \rangle = \chi_p \tag{37}$$

Thus, here the thermal susceptibility agrees exactly with the corresponding percolation property, provided the largest cluster is included in the summation in Eq. (37) or Eq. (2), respectively. It should be noted that Eq. (37) also holds for $T \leqslant T_c$ in finite systems, but gives the wrong thermodynamic limit.

As will be discussed in the next section, χ'_p in Eq. (36) and the term $N(\langle P_\infty^2 \rangle - \langle P_\infty \rangle^2)$ diverge with the same critical exponent as $T \to T_c$. Thus, we have χ' proportional to χ'_p, as requested. However, it is clear that the critical amplitudes of χ' and χ'_p differ, while they agree for χ and χ_p above T_c. But this implies that the universal ratios χ/χ' and χ_p/χ'_p must differ from each other.

4. NUMERICAL RESULTS AND FINITE-SIZE SCALING ANALYSIS

As a direct example that geometrical clusters are too large to describe magnetic correlations in an Ising model, Fig. 1 compares the pair connectedness function $c_{0,i}$ with the spin pair correlation function $\langle s_0 s_i \rangle$. It is seen that $c_{0,i}$ distinctly exceeds $\langle s_0 s_i \rangle$, while the pair connectedness func-

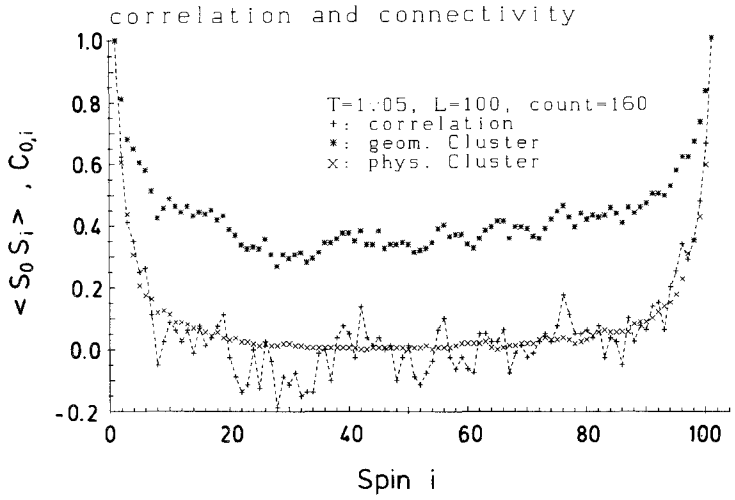

Fig. 1. Correlation function $\langle s_0 s_i \rangle$ versus distance i in a lattice direction of a 100×100 Ising lattice at $T = 1.05 T_c$ (+) as compared to the pair connectedness function of geometrical clusters (*) and of physical clusters (×).

tion for physical clusters as generated by the Swendsen–Wang algorithm is in good agreement with $\langle s_0 s_i \rangle$. At the same time, Fig. 1 shows that the description in terms of physical clusters works above T_c as well—previous numerical work on clusters[3,9,10–15,22] always has considered only $T < T_c$.

Figure 2a then compares the energy computed in two ways—directly as an expectation value of the Hamiltonian, and from the expectation value $\langle N_b \rangle$ of the number of bonds, using Eq. (24a). The excellent agreement between both approaches not only shows the consistency of our numerical procedures, but also means that the statistical effort is sufficient to reach a reasonable accuracy for this quantity. For the specific heat (Fig. 2b) also the results extracted from energy fluctuations are found to be consistent with the results from bond number fluctuations [Eq. (27)], though in this case just above T_c statistical errors lead to appreciable scatter.

Figure 3 compares the magnetization $\langle |M| \rangle$ and the percolation probability $\langle P_\infty \rangle$. As expected from Eq. (31), $\langle |M| \rangle$ and $\langle P_\infty \rangle$ are in quantitative agreement for T distinctly lower than T_c, while for $T \gtrsim T_c$ it is seen that $\langle |M| \rangle$ exceeds P_∞ distinctly. This clearly reflects the fact that many clusters contribute to $\langle |M| \rangle$ for $T > T_c$, not only the largest cluster that is measured by $\langle P_\infty \rangle$. In fact, the asymptotic finite-size dependence of $\langle |M| \rangle$ follows from the fact that the distribution of M for $T > T_c$ is a Gaussian distribution with width controlled by Eq. (37) and hence[22,30]

$$\langle |M| \rangle \sim L^{-d/2} = L^{-1}, \qquad L \to \infty, \quad T > T_c \tag{38}$$

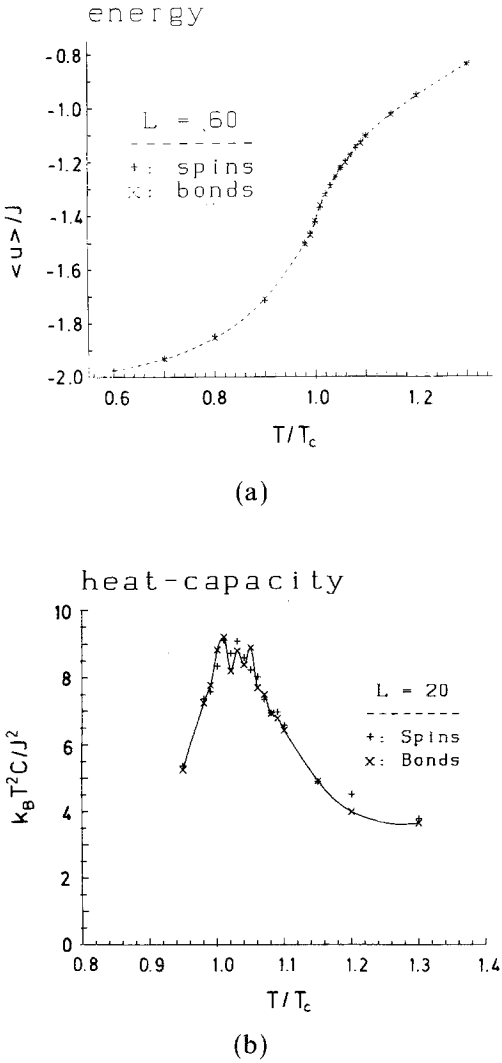

Fig. 2. (a) Internal energy (in units of the exchange) plotted versus temperature (in units of T_c) for a 60×60 lattice. (+) Expectation value of the Hamiltonian; (×) from Eq. (24a). (b) Normalized heat capacity $k_B T^2 C/J^2$ plotted versus T/T_c for a 20×20 lattice. (+) Result using C from energy fluctuations [Eq. (25)]; (×) resulting using C from bond number fluctuations [Eq. (27)].

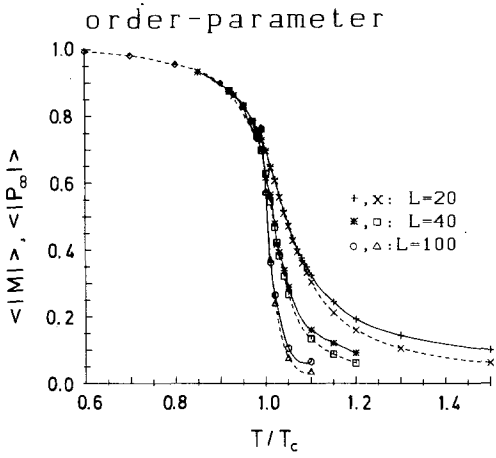

Fig. 3. Magnetization (—) and percolation probability (- -) plotted vs. T/T_c for three system sizes: $\langle |M| \rangle$ for (+) $L=20$, (*) $L=40$, and (○) $L=100$, and P_∞ is for (×) $L=20$, (□) $L=40$, and (△) $L=100$.

for $d=2$ dimensions, while the percolation probability can be shown to vanish according to a quicker variation with L, namely[31]

$$\langle P_\infty \rangle \sim L^{-d} \log L, \qquad L \to \infty, \quad T > T_c \tag{39}$$

Although both quantities $\langle |M| \rangle$ and $\langle P_\infty \rangle$ for the physical clusters are expected to exhibit finite-size scaling relations[30–35] of the same form,

$$\langle |M| \rangle = L^{-\beta/\nu} \tilde{M}(\varepsilon L^{1/\nu}), \qquad \varepsilon = T/T_c - 1 \tag{40a}$$

$$\langle P_\infty \rangle = L^{-\beta/\nu} \tilde{P}_\infty(\varepsilon L^{1/\nu}) \tag{40b}$$

the scaling functions $\tilde{M}$, $\tilde{P}_\infty$ must differ in order to reflect the two distinct asymptotic behaviors expressed in Eqs. (38), (39). Figure 4 presents a test of relations (40a) and (40b). Although finite-size scaling is reasonably well obeyed, one also recognizes systematic deviations due to corrections to finite-size scaling beyond the statistical scatter. High-precision data for much larger values of L would be required in order to provide clear numerical evidence for Eqs. (38), (39). This was outside the scope of our study.

Finally, we turn to the behavior of the susceptibilities χ' and $\chi'^{(p)}$ [Fig. 5; cf. Eqs. (35), (36)]. In this case the approximate result $\chi'^{(p)}$ expressed in terms of percolation properties only lies systematically above χ', because in the latter a systematically larger term ($\langle |M| \rangle^2 \geqslant \langle P_\infty \rangle^2$) is

subtracted. While near T_c both terms in Eq. (36) scale in the same way with system size, again their asymptotic behavior for large L at fixed $T > T_c$ is different: χ'_p goes to a finite constant, while[31]

$$N(\langle P_\infty^2 \rangle - \langle P_\infty \rangle^2) \sim L^{-d} \log^2 L, \qquad T > T_c \tag{41}$$

While the fluctuation of the largest cluster makes a significant contribution below T_c, it is rather unimportant above T_c (Fig. 6). Since both χ' and χ'_p for $T > T_c$ go to finite constants, the asymptotic behavior of the finite-size

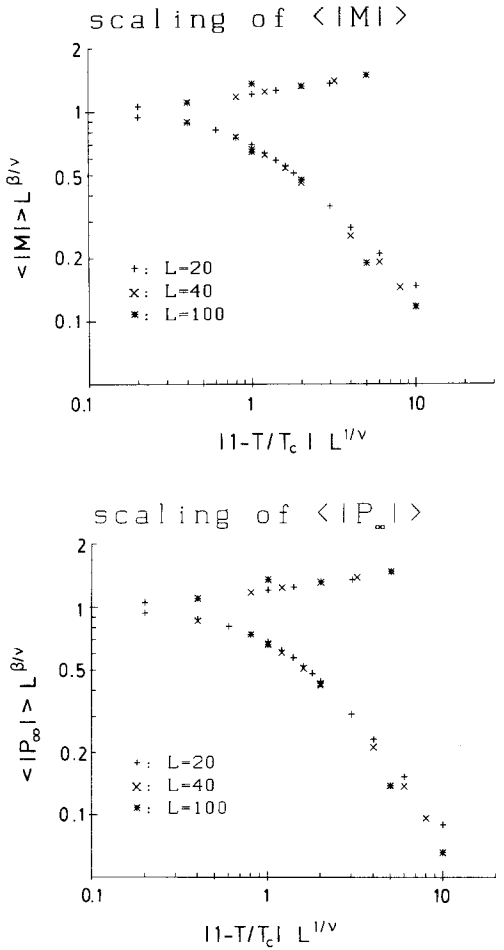

Fig. 4. Finite-size scaling plot of the magnetization (upper part) and of the percolation probability (lower part). The exponents used in the plot were the theoretical[8] values of the two-dimensional Ising model, $\beta = 1/8$, $\nu = 1$, as well as the exactly known[8] critical temperature. Same sizes as shown in Fig. 3 were used.

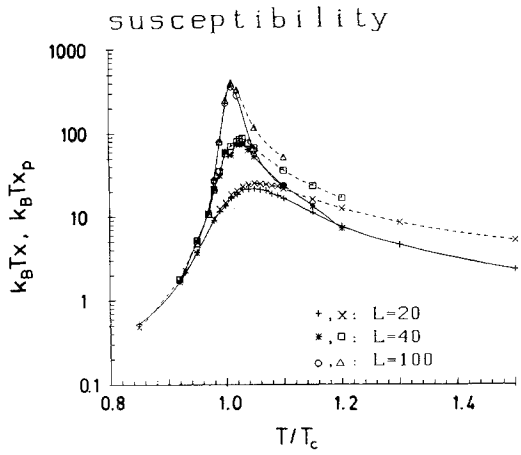

Fig. 5. Susceptibility $k_B T\chi'$, $k_B T\chi'^{(p)}$ (on a logarithmic scale) plotted vs. T/T_c for three system sizes. Full curves refer to χ' and broken curves to $\chi'^{(p)}$.

scaling functions $\tilde{\chi}'$, $\tilde{\chi}'^{(p)}$ defined by the following finite-size scaling relation is qualitatively the same, although the functions themselves again differ:

$$k_B T\chi' = L^{-\gamma/\nu}\tilde{\chi}'(\varepsilon L^{1/\gamma}) \tag{42a}$$

$$k_B T\chi'^{(p)} = L^{-\gamma/\nu}\tilde{\chi}'^{(p)}(\varepsilon L^{1/\gamma}) \tag{42b}$$

A check of these relations is provided in Fig. 7. Of course, a similar scaling relation can also be studied for $k_B T\chi$ [Eq. (37)], but this is omitted here.

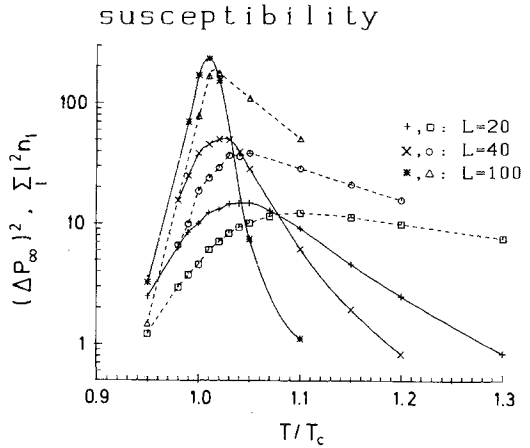

Fig. 6. Normalized fluctuation $(\Delta P)^2 \equiv N(\langle P_\infty^2\rangle - \langle P_\infty\rangle^2)$ of the largest cluster (full curves) and second moment of the cluster distribution $\{\sum l^2 n_l \equiv \sum'_{m_{cl}} m_{cl}^2 < p'(m_{cl}) = \chi'_p\}$ (broken curves) plotted vs. T/T_c.

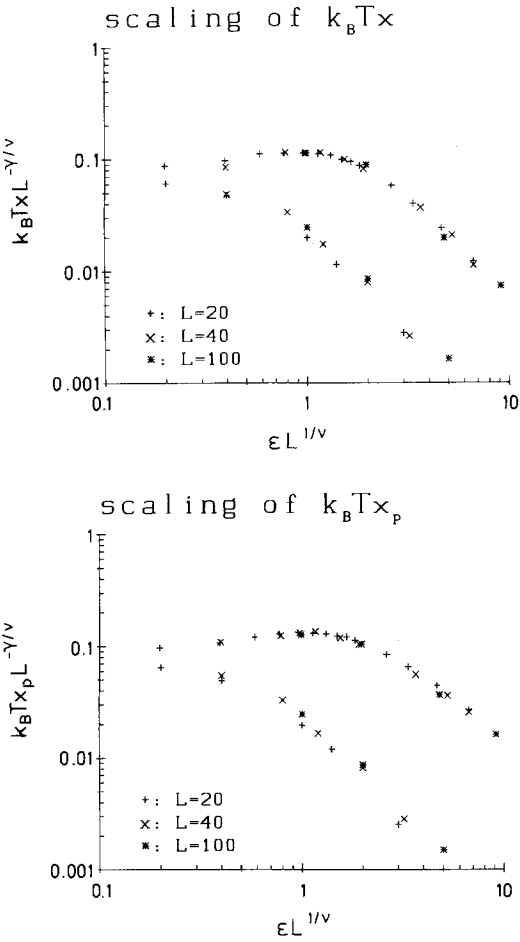

Fig. 7. Finite-size scaling plot of $k_B T\chi'$ (upper part) and $k_B T\chi'^{(p)}$ (lower part). Again theoretical values for the Ising critical exponents ($\nu = 1$, $\gamma = 7/4$) and for T_c were used.

5. THE CLUSTER SIZE DISTRIBUTION

In this section the numerical results on the cluster size distribution $n_l = p(m_{cl} = l) + p(m_{cl} = -l)$ are presented. Again it is useful in each configuration to split off the contribution of the largest cluster, whose size is denoted as l_∞,

$$n_l = n'_l + \frac{1}{N}\delta_{l,l_\infty} \tag{43}$$

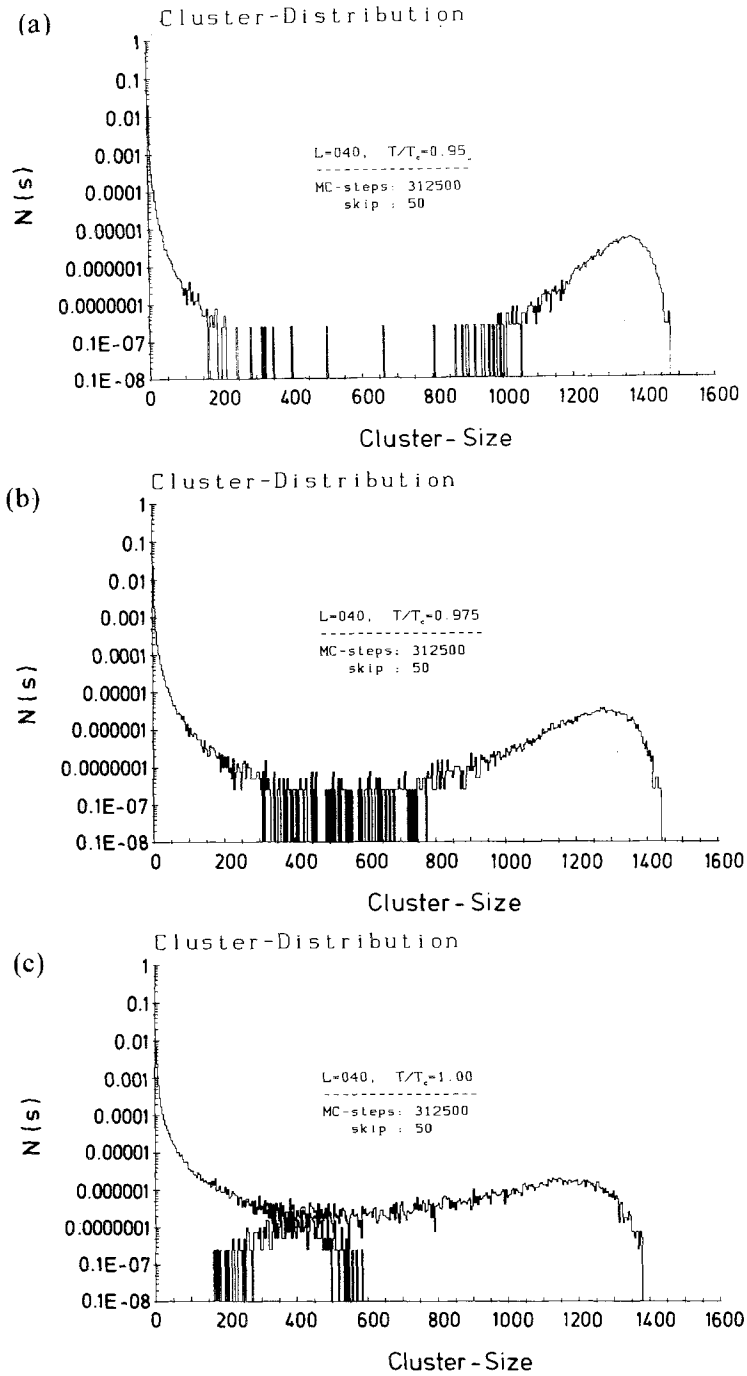

Fig. 8. Cluster size distribution $\bar{n}_l$ vs. l for $L=40$ and various temperatures: $T/T_c=0.95$ (a), 0.975 (b), 1.00 (c). Four consecutive values of l are averaged together. After omission of the first 1000 MCS, averages were based on 6250 configurations taken at "time" intervals of $\delta t=50$ MCS.

Taking an ensemble average, the size l_∞ of the largest cluster fluctuates from one configuration to the next, of course, and thus from the average of the Kronecker symbol we obtain a continuous function $\bar{n}_l^\infty$ such that

$$\bar{n}_l = \bar{n}_l' + \bar{n}_l^\infty \tag{44}$$

While at temperatures $T > T_c$ both distributions $\bar{n}_l'$, $\bar{n}_l^\infty$ strongly overlap each other, for $T < T_c$ they are rather clearly separated, at least for large enough linear dimensions L (Figs. 8–10). Additional such data for $L = 20$

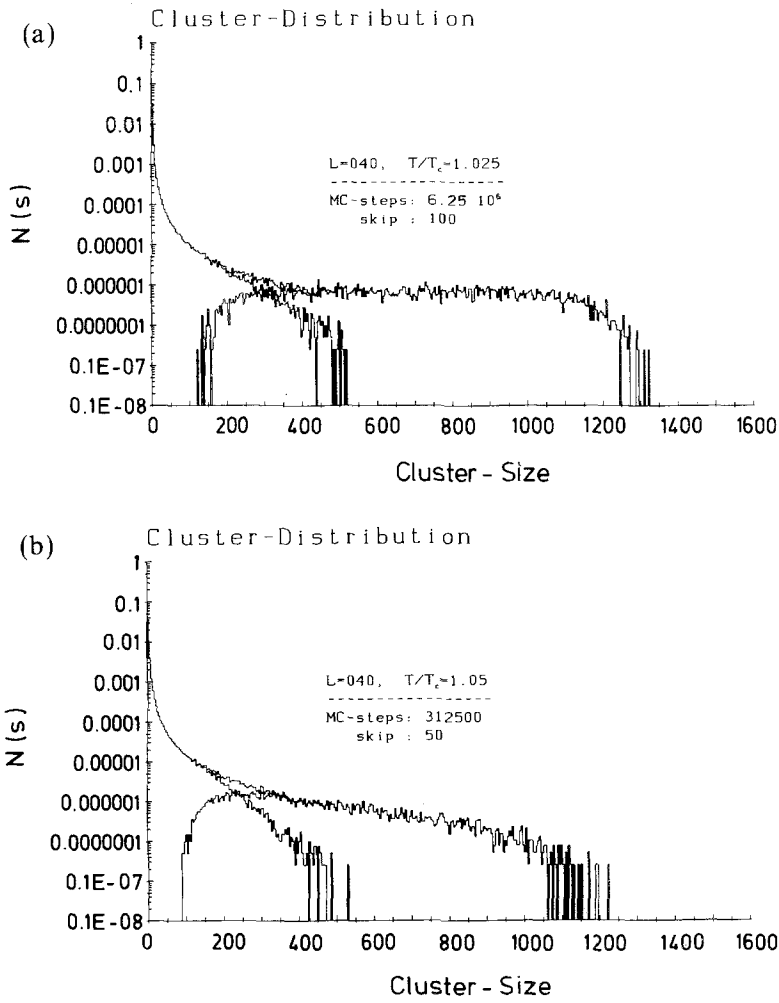

Fig. 9. Same as Fig. 8, but for $T/T_c = 1.025$ (a) and 1.05 (b).

are displayed in ref. 25. Of course, the first moment of the distribution $\bar{n}_l^\infty$ is related to the percolation probability $\langle P_\infty \rangle$ as

$$\langle P_\infty \rangle = \sum_l l\bar{n}_l^\infty = \bar{l}^\infty / N \tag{45}$$

It is interesting to note that the distribution $\bar{n}_l^\infty$ is distinctly non-Gaussian. From the discussion of the finite-size behavior of $\langle P_\infty \rangle$ in the previous section we immediately conclude (for $N = L^d$)

$$\bar{l}^\infty \sim L^d, \qquad T < T_c \tag{46a}$$

$$\bar{l}^\infty \sim L^{d-\beta/\nu}, \qquad T = T_c \tag{46b}$$

$$\bar{l}^\infty \sim \log L, \qquad T > T_c \tag{46c}$$

The width of the distribution $\bar{n}_l^\infty$ is given by the fluctuations of the percolation probability

$$\overline{\Delta l}^\infty = \left[\sum_l l^2 \bar{n}_l^\infty - \left(\sum_l l\bar{n}_l^\infty \right)^2 \right]^{1/2} = L^{d/2} [N(\langle P_\infty^2 \rangle - \langle P_\infty \rangle^2)]^{1/2} \tag{47}$$

From the finite size-behavior of χ_p and Eq. (41) we conclude

$$\overline{\Delta l}^\infty \sim L^{d/2}, \qquad T < T_c \tag{48a}$$

$$\overline{\Delta l}^\infty \sim L^{(d+\gamma/\nu)/2} = L^{d-\beta/\nu}, \qquad T = T_c \tag{48b}$$

$$\overline{\Delta l}^\infty \sim \log L, \qquad T > T_c \tag{48c}$$

Combining Eqs. (46) and (48), we see that the relative error of the percolation probability (or, equivalently, the mean size $\bar{l}^\infty$ of the largest cluster) is independent of L for $T \geqslant T_c$:

$$\frac{\overline{\Delta P}_\infty}{\langle P_\infty \rangle} = \frac{\overline{\Delta l}^\infty}{\bar{l}^\infty} \sim \begin{cases} \text{const}, & T \geqslant T_c \\ L^{-d/2}, & T < T_c \end{cases} \tag{49a, 49b}$$

Thus, $\langle P_\infty \rangle$ (or $\bar{l}^\infty$) are "strongly self-averaging"[22,36] for $T < T_c$ only, while for $T \geqslant T_c$ complete lack of self-averaging is exhibited. This fact is responsible for the lack of narrowing of $\bar{n}_l^\infty$ for $T \geqslant T_c$ with increasing size.

While the shape of the distribution $\bar{n}_l^\infty$ changes dramatically as T increases from $T < T_c$ to $T > T_c$ [for $T < T_c$ it asymptotically becomes a Gaussian; cf. Eq. (49b) and Fig. 10a; notice also the pronounced flatness of the $\bar{n}_l^\infty$ vs. l curves just above T_c], the distribution $\bar{n}_l'$ shows much less structure; it is a monotonically decreasing function of cluster size both below T_c, above T_c, and right at T_c. Previous work[3,9,18] has usually

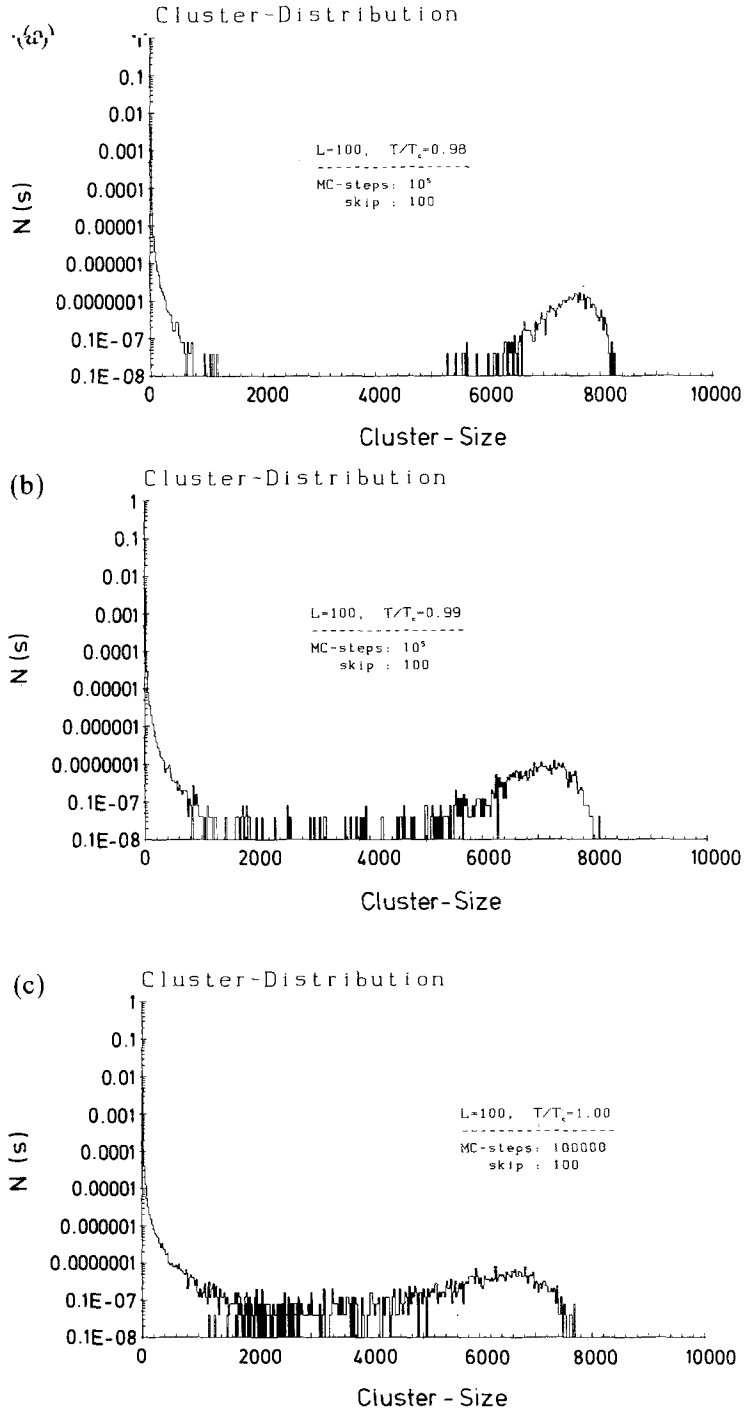

Fig. 10. Cluster size distribution $\bar{n}_l$ vs. l for $L = 100$ and various temperatures: $T/T_c = 0.98$ (a), 0.99 (b), 1.00 (c), 1.01 (d), and 1.02 (e). Twenty-five consecutive values of l are averaged together. After omission of the first 1000 MCS, averages were based on 1000 configurations taken at "time" intervals of $\delta t = 100$ MCS.

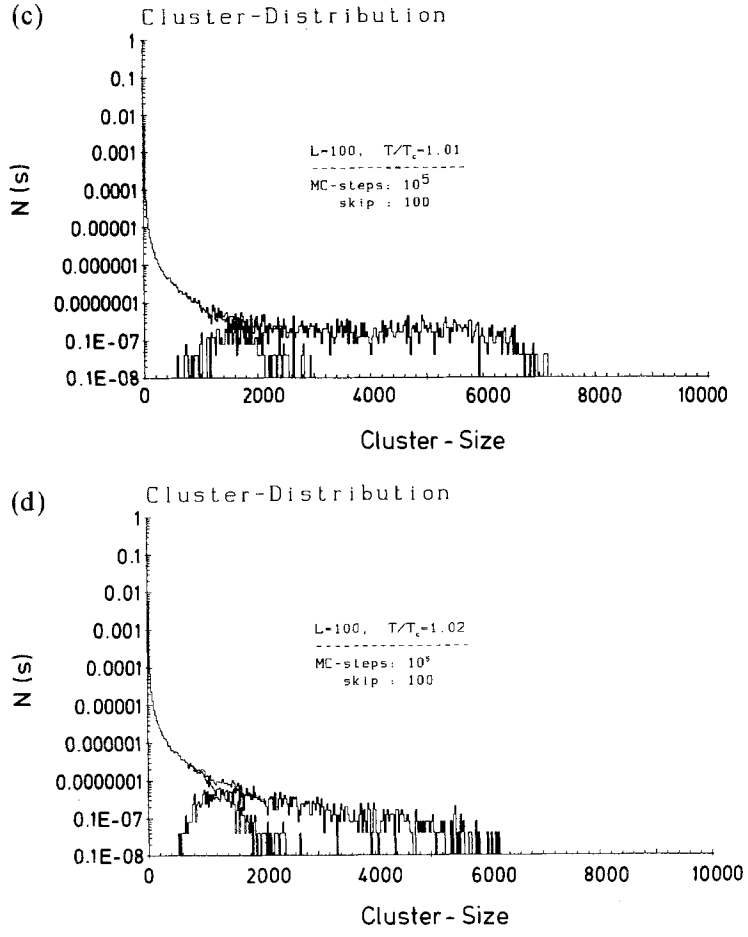

Fig. 10. (*Continued*)

discussed only $\bar{n}_l'$ for $T \leqslant T_c$, mostly applying the inappropriate geometrical cluster definition.

We now turn to the finite-size scaling description of the cluster size distributions $\bar{n}_l^{\infty}$ and $\bar{n}_l'$, respectively:

$$\bar{n}_l^{\infty}(T, L) = L^{-(2d-\beta/\nu)}\tilde{n}^{\infty}\{lL^{-(d-\beta/\nu)}, \varepsilon L^{1/\nu}\} \tag{50a}$$

$$\bar{n}_l'(T, L) = L^{-(2d-\beta/\nu)}\tilde{n}'\{lL^{-(d-\beta/\nu)}, \varepsilon L^{1/\nu}\} \tag{50b}$$

where $\tilde{n}^{\infty}, \tilde{n}'$ are suitable scaling functions, which now depend on two arguments. While the argument $\varepsilon L^{1/\nu}$ is of course the standard argument

appearing in finite-size scaling functions,[30–35] the other argument $lL^{-(d-\beta/\nu)}$ needs comment. Here we have invoked the principle that at T_c all cluster sizes scale with L in the same way and hence also in the same way as $\bar{l}^{\infty}$, for which we know already that $\bar{l}^{\infty} \sim L^{d-\beta/\nu}$ [Eq. (46b)]. Since in each configuration there is just one largest cluster l^{∞} [Eq. (43)], we have the normalization

$$1 = N \sum_{l} \bar{n}_l^{\infty} = L^d \int_0^{\infty} dl\, \bar{n}_l^{\infty} = \int_0^{\infty} d\xi\, \tilde{n}^{\infty}(\xi, \varepsilon L^{1/\nu}) \tag{51}$$

Since $\bar{n}_l^{\infty}$ vanishes for large L both for $l \to 0$ and for $l \to \infty$, and the main contribution comes from values of l which are of the same order as the (large) number $\bar{l}^{\infty}$, we could replace the summation in Eq. (51) by an integral with negligible error. Equation (51) fixes the prefactor as $L^{-(2d-\beta/\nu)}$ in Eq. (50a). We then make the further assumption that $\bar{n}_l^{\infty}$ and $\bar{n}_l'$ should scale in the same way, and thus obtain Eq. (50b). In order to make contact with the more traditional scaling theories for clusters,[3] we define the exponents τ, σ as follows:

$$\tau = 2 + 1/\delta, \qquad \sigma = 1/(\beta\delta) \tag{52}$$

and note that the exponents used in Eq. (50) can be rewritten in terms of τ, σ as follows:

$$2d - \beta/\gamma = \tau/(\nu\sigma), \qquad d - \beta/\nu = 1/(\nu\sigma) \tag{53}$$

Therefore, Eqs. (50a), (50b) can also be written as follows, redefining suitably the homogeneous functions:

$$\begin{aligned} \bar{n}_l^{\infty}(T, L) &= L^{-\tau/(\nu\sigma)} \tilde{n}^{\infty}\{lL^{-1/\nu\sigma}, \varepsilon L^{1/\nu}\} \\ &= l^{-\tau} \tilde{\tilde{n}}^{\infty}\{\varepsilon l^{\sigma}, l^{\sigma}/L^{1/\nu}\} \end{aligned} \tag{54a}$$

$$\begin{aligned} \bar{n}_l'(T, L) &= L^{-\tau/(\nu\sigma)} \tilde{n}'\{lL^{-1/\nu\sigma}, \varepsilon L^{1/\nu}\} \\ &= l^{-\tau} \tilde{\tilde{n}}'\{\varepsilon l^{\sigma}, l^{\sigma}/L^{1/\nu}\} \end{aligned} \tag{54b}$$

In the limit $L \to \infty$ where the second argument of $\tilde{\tilde{n}}^{\infty}$, $\tilde{\tilde{n}}'$ vanishes, Eqs. (54a), (54b) take exactly the form postulated in ref. 3. Note, however, that while we expect $\tilde{\tilde{n}}'(\varepsilon l^{\sigma}, 0)$ to exist, one must not put the argument $l^{\sigma}/L^{1/\nu}$ equal to zero in $\tilde{\tilde{n}}^{\infty}$, since this function is singular in the limit $L \to \infty$, in order to yield Eq. (46b).

The temperatures in Figs. 8–10 were chosen such that finite-size scaling can be studied for five choices of $\varepsilon L^{1/\nu} = \varepsilon L$, namely $\varepsilon L = \pm 2, \pm 1$, and 0. Figures 11–15 suggest that the scaling relations (50a), (50b), (54a), (54b)

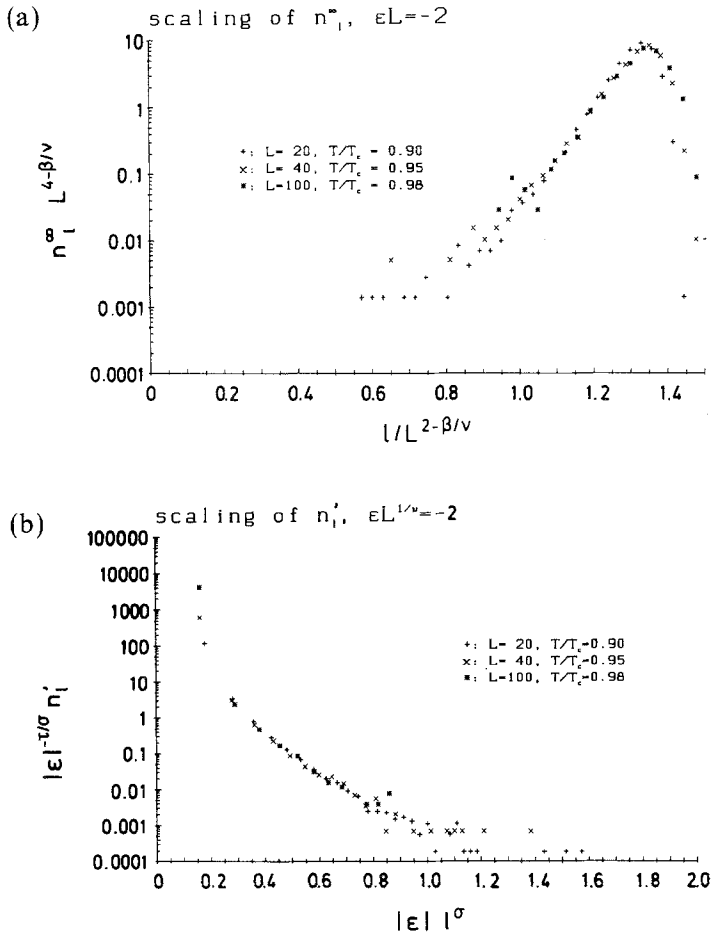

Fig. 11. Finite-size scaling plot of the cluster size distributions (a) $\bar{n}_l^{\infty}$ and (b) $\bar{n}'_l$ for $\varepsilon L = -2$. Different symbols represent sizes and temperatures as indicated in the figure.

are indeed true! Note that for $\bar{n}_l^{\infty}$ we have used the variables of ordinate and abscissa in Figs. 11a–15a appropriate for Eq. (50a), while for $\bar{n}'_l$ we have chosen a form equivalent to Eq. (54b), namely $\bar{n}'_l(T, L) = |\varepsilon|^{\tau/\sigma}\, \tilde{N}'(\varepsilon l^{\sigma}, \varepsilon L^{1/\nu})$, apart from the case $\varepsilon = 0$, where variables according to Eq. (54b) were chosen (Fig. 13b). This figure shows systematic deviations from finite-size scaling for very small l, while for large l, statistical scatter sets in.

There are various attempts to describe the distribution function n'_l. According to the Fisher[1] droplet model, $n'_l \sim l^{-\tau} \exp(-\text{const}\, |\varepsilon|\, l^{\sigma})$. Thus,

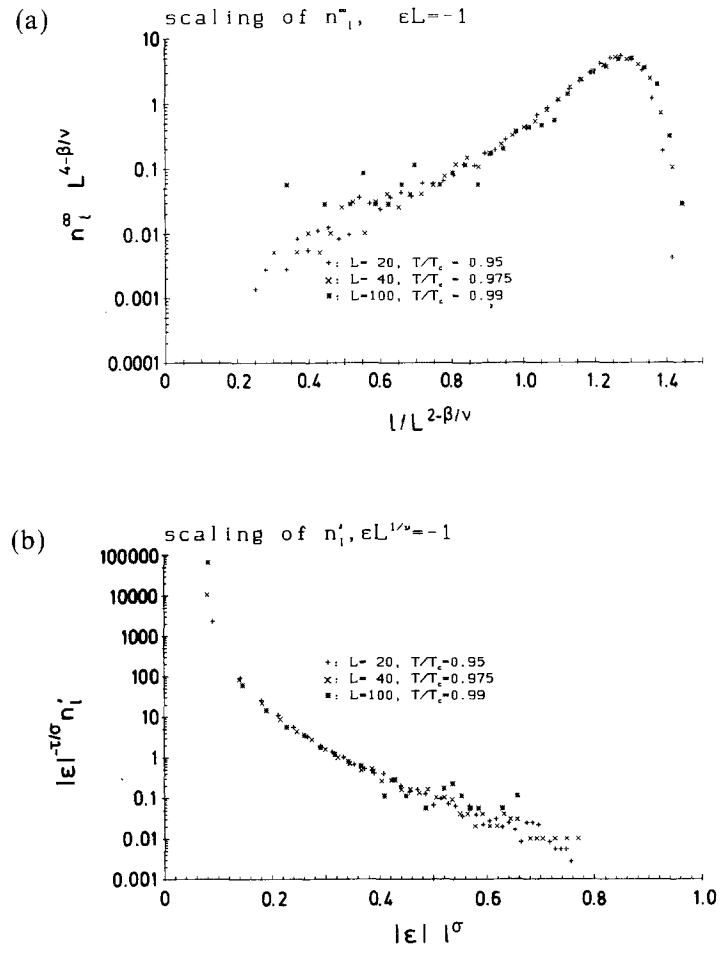

Fig. 12. Same as Fig. 11, but for $\varepsilon L = -1$.

in a plot of $\log(n_l')$ versus εl^{σ} (Figs. 11b, 12b) one should see a straight line for large l. Although the data are roughly consistent with such a behavior, the strong statistical scatter present for large $|\varepsilon|\, l^{\sigma}$ prevents us from making strong statements about this problem. For $T > T_c$, on the other hand, arguments exist[3,17] which imply that $\log(n_l') \sim l$ for large l. This implies that on a plot of $\log(n_l')$ vs. εl^{σ} one should see a distinct downward curvature, and this is in fact seen in Fig. 15b for large εl^{σ}.

For $\varepsilon < 0$ ($T < T_c$) and $|\varepsilon|\, L \to \infty$ we expect that asymptotically (for $l \to \infty$) the distribution $\bar{n}_l'$ can be interpreted as $\bar{n}_l' \sim \exp(-\Delta F_l / k_B T)$,

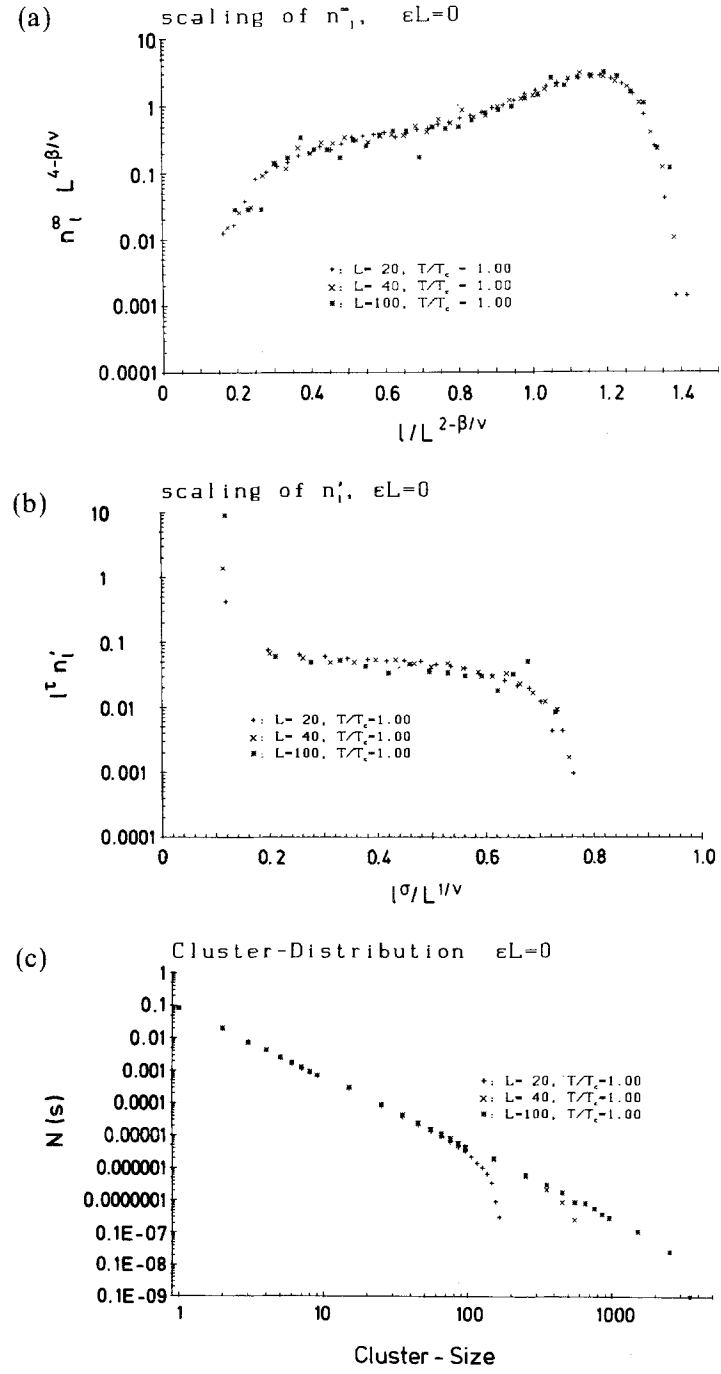

Fig. 13. Same as Fig. 11, but for $\varepsilon L = 0$. In addition, part (c) presents a simple (unscaled) plot of $\bar{n}_l'$ vs. l for $\varepsilon = 0$ and three values of L, to show the approach toward a simple power law, $\bar{n}_l' \sim l^{-\tau}$.

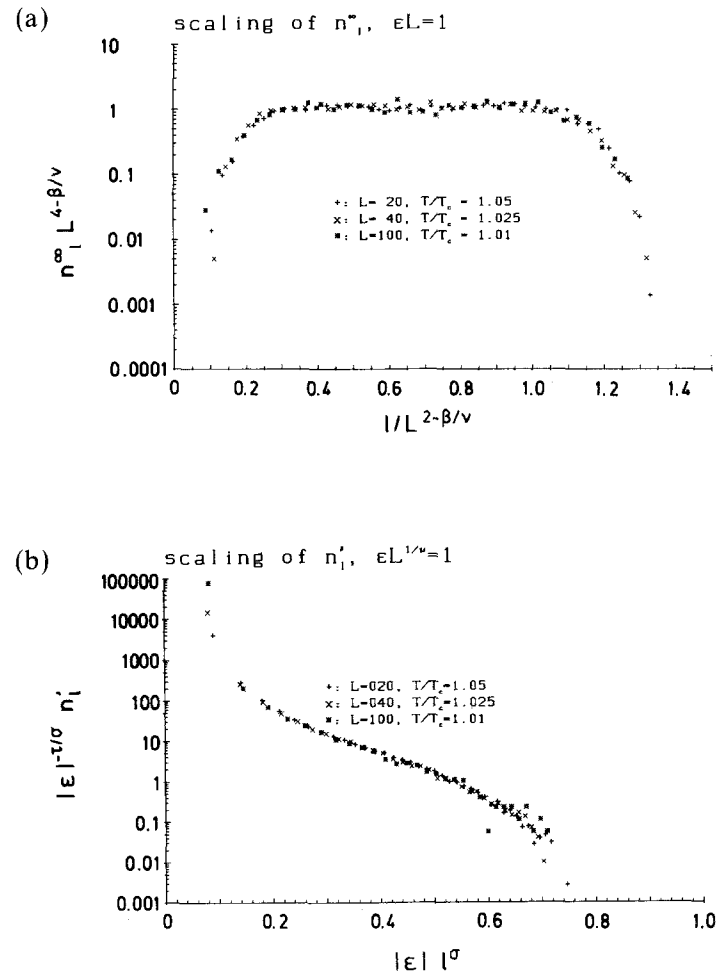

Fig. 14. Same as Fig. 11, but for $\varepsilon L = +1$.

where ΔF_l is the formation free energy of a droplet, which (in the absence of a magnetic field, i.e., at the coexistence curve of the Ising model) should be describable basically by a surface free energy of the droplet, i.e., surface area times surface tension.[3] This regime is only reached if clusters are studied whose linear dimensions are much larger than the correlation length. A substantially larger statistical effort than available here would be needed for such a study. The present study has taken about 100 hr CPU time on a Siemens 7561 scalar computer.

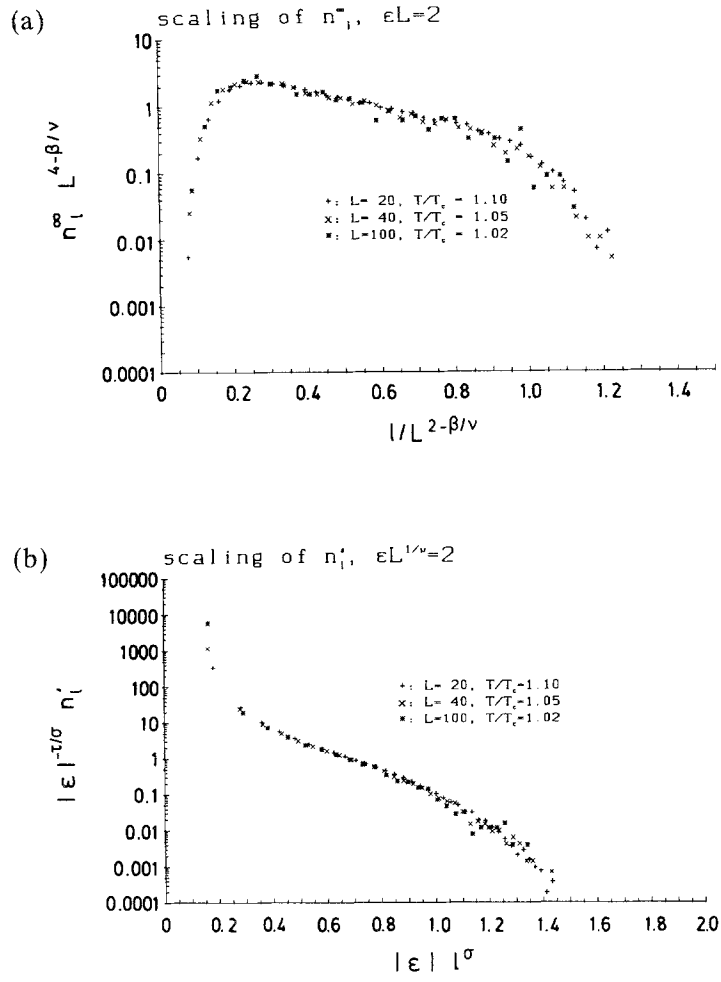

Fig. 15. Same as Fig. 11, but for $\varepsilon L = +2$.

6. CONCLUSIONS

In this paper the Swendsen–Wang algorithm[23] for the two-dimensional Ising model was applied to study the physical clusters near the critical point. The justification of the algorithm in terms of the Fortuin–Kasteleyn mapping to correlated percolation problems is used as a starting point to derive fluctuation relations for specific heat and susceptibility in terms of cluster properties, and a comparative study of the finite-size effects

on percolation probability and magnetic order parameter is presented. While these two quantities coincide in the thermodynamic limit, finite-size corrections are systematically different. In contrast, the magnetic susceptibility below T_c differs from the corresponding percolation susceptibility even in the thermodynamic limit, due to a contribution expressing fluctuations in the magnetic moment of the percolating cluster. These general considerations are explicitly illustrated by detailed Monte Carlo results; while finite-size scaling of thermal properties for the Ising model has been studied in detail before, our corresponding results for the associated correlated percolation problem are new. The resulting scaling functions are estimated numerically and show all expected general properties.

The main result of the present paper is the detailed analysis of the size distribution of the physical clusters. Both the distribution function of the largest cluster—which below T_c represents the percolating network—and the distribution of the remaining finite clusters are studied. Both distribution functions are consistent with finite-size scaling and with thermal scaling, providing thus the first clear evidence for scaling hypotheses in terms of clusters, which were proposed more than 12 years ago, but have not yet been tested so far. Our results on the cluster distributions include data for both below and above T_c, but are for zero external magnetic field only.

Clearly a crucial point for the feasibility of this study was the strong reduction of critical slowing down provided by the algorithm: Since the relaxation time only increases much more slowly than the standard single spin-flip kinetic Ising model[23,40] even for $L = 100$, it suffices to skip $\delta t = 50$ steps between successive configurations used in the averaging in order that they are uncorrelated. Thus, significant statistical effort on the cluster size distribution was possible with moderate effort.

Of course, it would be desirable to include the magnetic field into the problem and to study much larger values of L, as in the standard random percolation problem,[7] in order to obtain results of very high precision. Another very desirable extension concerns work on problems with quenched-in randomness, where critical slowing down is even more severe.[37]

ACKNOWLEDGMENTS

This work was partially supported by the Deutsche Forschungsgemeinschaft, Sonderforschungsbereich 262. Particular thanks are due to a referee whose suggestions were instrumental to the formulation of the FKSW algorithm presented in Section 2, and for numerous other helpful comments.

REFERENCES

1. M. E. Fisher, *Physics* **3**:267 (1967).
2. C. S. Kiang and D. Stauffer, *Z. Phys.* **235**:130 (1970); A. Eggington, C. S. Kiang, D. Stauffer, and G. H. Walker, *Phys. Rev. Lett.* **26**:820 (1971); D. Stauffer, C. S. Kiang, and G. H. Walker, *J. Stat. Phys.* **3**:323 (1971).
3. K. Binder, *Ann. Phys.* **98**:390 (1976).
4. A. Coniglio and W. Klein, *J. Phys. A* **13**:2775 (1980).
5. A. Coniglio, C. R. Nappi, F. Peruggi, and L. Russo, *Commun. Math. Phys.* **51**:315 (1976).
6. C.-K. Hu, *Phys. Rev. B* **29**:5103 (1984).
7. D. Stauffer, *Introduction to Percolation Theory* (Taylor and Francis, London, 1985).
8. B. M. McCoy and T. T. Wu, *The Two-Dimensional Ising Model* (Harvard University Press, Cambridge, Massachusetts, 1968).
9. E. Stoll, K. Binder, and T. Schneider, *Phys. Rev. B* **6**:2777 (1972).
10. K. Binder and D. Stauffer, *J. Stat. Phys.* **6**:49 (1972).
11. H. Müller-Krumbhaar, *Phys. Lett.* **48A**:459 (1974).
12. D. W. Heermann and D. Stauffer, *Z. Physik B* **44**:339 (1981).
13. H. Müller-Krumbhaar and E. P. Stoll, *J. Chem. Phys.* **65**:4294 (1974).
14. A. Marro and J. Toral, *Physica* **122A**:563 (1983).
15. M. Nauenberg and J. Cambier, in *Fractals in Physics*, L. Pietronero and E. Tosatti, eds. (North-Holland, Amsterdam, 1986), p. 421.
16. M. F. Sykes and D. S. Gaunt, *J. Phys. A* **9**:2131 (1976).
17. K. Binder, D. Stauffer, and H. Müller-Krumbhaar, *Phys. Rev. B* **12**:5261 (1975); R. Kretschmer, K. Binder, and D. Stauffer, *J. Stat. Phys.* **15**:267 (1976).
18. K. Binder and D. W. Heermann, in *Scaling Phenomena in Disordered Systems*, R. Pynn and A. Skjeltorp, eds. (Plenum Press, New York, 1985), p. 227.
19. K. Binder (ed.), *Monte Carlo Methods in Statistical Physics*, 2nd ed. (Springer, Berlin, 1986).
20. D. W. Heermann, *Computer Simulation Methods in Theoretical Physics* (Springer, Berlin, 1976).
21. K. Binder (ed.), *Applications of the Monte Carlo Method in Statistical Physics*, 2nd ed. (Springer, Berlin, 1987).
22. K. Binder and D. W. Heermann, *Monte Carlo Simulation in Statistical Physics: An Introduction* (Springer, Berlin, 1988).
23. R. H. Swendsen and J. S. Wang, *Phys. Rev. Lett.* **58**:86 (1987).
24. P. W. Kasteleyn and C. M. Fortuin, *J. Phys. Soc. Japan* **26**(Suppl.):11 (1969); C. M. Fortuin and P. W. Kasteleyn, *Physica* **57**:536 (1972); C. M. Fortuin, *Physica* **58**:393, **59**:545 (1972).
25. M. D'Onorio de Meo, Diplomarbeit, Universität Mainz (1988), unpublished.
26. J. Hoshen and R. Kopelman, *Phys. Rev. B* **27**:3438 (1976).
27. S. Wansleben, *Comput. Phys. Commun.* **43**:9 (1987).
28. N. Ito and Y. Kanada, *Supercomputer* **25**:31 (1988).
29. A. H. Burkitt and D. W. Heermann, *Comput. Phys. Commun.* **54**:201 (1989).
30. K. Binder, *Z. Physik B* **43**:119 (1981).
31. A. Margolina and H. J. Herrmann, *Phys. Lett.* **104A**:295 (1984).
32. M. E. Fisher, in *Critical Phenomena*, M. S. Green, ed. (Academic Press, New York, 1971), p. 1.
33. M. E. Fisher and M. N. Barber, *Phys. Rev. Lett.* **28**:1518 (1972).
34. M. N. Barber, in *Phase Transitions and Critical Phenomena*, Vol. 8, C. Domb and J. L. Lebowitz, eds. (Academic Press, New York, 1983), p. 145.

35. K. Binder, *Ferroelectrics* **43**:73 (1987).
36. A. Milchev, K. Binder, and D. W. Heermann, *Z. Physik B* **63**:527 (1986).
37. R. Gissler, D. W. Heermann, and A. H. Burkitt, work in progress.
38. R. G. Edwards and A. D. Sokal, *Phys. Rev. D* **38**:2009 (1988).
39. N. Ito, M. Taiji, and M. Suzuki, *J. Phys. (Paris)* **C8**(Suppl. 12):1397 (1988).
40. D. W. Heermann and A. H. Burkitt, *Physica A* **162**:210 (1990).
41. D. W. Heermann, A. H. Burkitt, and J. Kertesz, to be published.